Structural Durability & Health Monitoring

Tech Science Press

https://doi.org/10.32604/sdhm.2026.075555

ARTICLE

Analysis of the Comprehensive Structural System of the Three-Tower Cable-Stayed Bridge

Dawei Shen[1], Xiang Chen[1], Yuanyin Song[2,*], Yaoyu Zhu[2], Deyun Liu[2], Rong Lv[1] and Wen-Wei Wang[3]

[1]Guangdong Provincial Highway Construction Co., Ltd., Guangzhou, China
[2]CCCC Highway Bridges National Engineering Research Center Co., Ltd., Beijing, China
[3]School of Transportation, Southeast University, Nanjing, China

*Corresponding Author: Yuanyin Song. Email: songyuanyin@bnerc.com

Received: 04 November 2025; Accepted: 02 March 2026; Published: 30 June 2026

ABSTRACT: This study systematically investigates the static and dynamic performance of the comprehensive structural system for the Huangmaohai extra-long-span three-tower cable-stayed bridge. A full-bridge finite element model was developed, incorporating elastic restraints at the central tower, viscous dampers at the side towers, and transverse seismic isolation bearings. Detailed structural parameters and loading conditions are provided. Subsequently, a systematic analysis was conducted on the structural stiffness, internal forces in the bearings, and stresses in the main girder and stay cables under static loads, thereby verifying the structural safety during both the completed bridge state and operational phase. Finally, through dynamic characteristic and seismic response analyses, the internal forces and displacement responses of the bridge towers in the baseline model and the comprehensive model under E1 and E2 seismic actions were compared. The results indicate that the proposed comprehensive structural system effectively controls main girder stresses, enhances structural stiffness, and significantly reduces seismic-induced internal forces. This research provides crucial technical bearing for the design and seismic optimization of similar extra-long-span cable-stayed bridges.

KEYWORDS: Cable-stayed bridge; static characteristics; dynamic characteristics; seismic response; finite element model

1 Introduction

Cable-stayed bridges, recognized for their substantial spanning capacity and adaptability to diverse topographical conditions, represent one of the primary structural types for long-span bridges [1–3]. With rapid economic development, the demand for crossing large rivers and valleys has driven significant advancements in cable-stayed bridge technology, leading to the construction of numerous super-long-span cable-stayed bridges [4–6]. However, as the length of the bridge increases, the impact of certain disasters or accidents, such as earthquakes, typhoons, and ship collisions, on the bridge will significantly increase [7–9]. For cable systems, failures caused by factors such as fatigue and corrosion also impose higher demands on bridge constructors [10–12]. This requires us to further ensure the safety and rationality of the overall structural design of the bridge.

A cable-stayed bridge primarily consists of three components: the girder, towers, and stay cables. Mechanically, the main girders are subjected to combined bending moments and axial forces. For spans exceeding 600 m, steel truss girders or steel box girders are predominantly employed. Long-span steel

box girder cable-stayed bridges are highly statically indeterminate structures [13], offering advantages such as long spans, lightweight yet high strength, and construction efficiency [14–16]. Furthermore, they demonstrate superior performance in service life, construction speed, maintenance management, and economic efficiency [17,18]. The towers, functioning primarily in compression, are typically constructed from concrete to utilize its high compressive strength, substantial stiffness, and cost-effectiveness [19,20]. The girder sections often utilize closed steel box designs, while the tower sections are generally made of concrete box structures. Stay cables commonly consist of parallel high-strength steel wires or strands [21–23]. During bridge construction and service, variable actions such as vehicle loads, wind loads, and thermal effects must be comprehensively considered, as these constitute critical load cases in bridge design [24–26].

Extensive research has been conducted on the static and dynamic characteristics of cable-stayed bridges. Hiroshi et al. [27] applied the updated Lagrangian formulation and discretized the towers using closed box sections, analyzing the ultimate bearing capacity during construction and service stages by considering material nonlinearity while neglecting shear deformation. Qiu et al. [28] investigated static and dynamic behavior of a cable-stayed bridge with main span of 1800 m, examining the influence of parameters such as the rise-span ratio, the suspension-to-span ratio, the constraint condition of the stiffened girder, the number of auxiliary piers at side spans, the layout of suspension cables, and the elastic modulus of suspension cables. To reduce the internal stresses in the bridge towers and main girders, cable-stayed bridges employ floating or semi-floating systems. However, this results in insufficient longitudinal restraint of the main girders, necessitating the use of devices such as isolation bearings or elastic restraints to limit longitudinal displacement. Xu et al. proposed a novel vibration control system to constrain the longitudinal displacement of the levitation system based on the traditional tuned viscous mass damper and negative stiffness amplifying damper [29].

This paper systematically studies the static and dynamic structural performance of the Huangmaohai Bridge, focusing on optimizing the comprehensive system for the distribution of internal forces within the bridge, thereby ensuring more reasonable stress during service and enhancing the bridge's resistance under seismic effects. A finite element model is established to analyze structural stiffness, bearing internal forces, and stresses in the main girder and stay cables under various service conditions. Furthermore, dynamic characteristics and seismic responses are examined, comparing the internal forces and displacement responses of the towers in the baseline model and the comprehensive model under E1 and E2 seismic events. This research provides valuable technical references for the design and seismic optimization of similar super-long-span cable-stayed bridges.

In the section on research gaps and contributions, this research confirms that the static performance of the Huangmaohai Bridge meets the code requirements and demonstrates the structural rationality. It also shows that the integrated structural system significantly enhances seismic performance, providing a viable seismic resistance strategy for long-span cable-stayed bridges. However, the finite element model used in this research simplifies the boundary and damping conditions, which require further investigation. Additionally, the performance of the integrated structural system under other types of disasters needs to be further validated.

2 Engineering Background

The Huangmaohai extra-long-span three-tower cable-stayed bridge is recognized as the largest span bridge of its type both domestically and internationally, and is characterized by its innovative structural design. The structure is configured with single-column towers, separated steel box girders, and a spatial cable system with dual cable planes, while high aesthetic requirements are also imposed. The variable-cross-section and irregular tower shapes result in complex structural forces and significant construction challenges.

The Huangmaohai Bridge is designed with a span arrangement of 100 + 280 + 2 × 720 + 280 + 100 m as a steel box girder cable-stayed bridge. The main girder is composed of two separate steel boxes connected by transverse cross girders. Parallel wire cables are employed, and vibration dampers are installed on the stay cables. The towers are constructed as concrete single-column structures. The pile caps are designed with circular shapes, while the transition piers and auxiliary piers are configured as full-width T-shaped sections. A rendering of the completed bridge is shown in Fig. 1. Key design issues are addressed through systematic and structural innovations aimed at enhancing the vertical stiffness of the main girder, optimizing thermal stress distribution, achieving superior overall bridge performance, and ensuring economic efficiency in component dimensions.

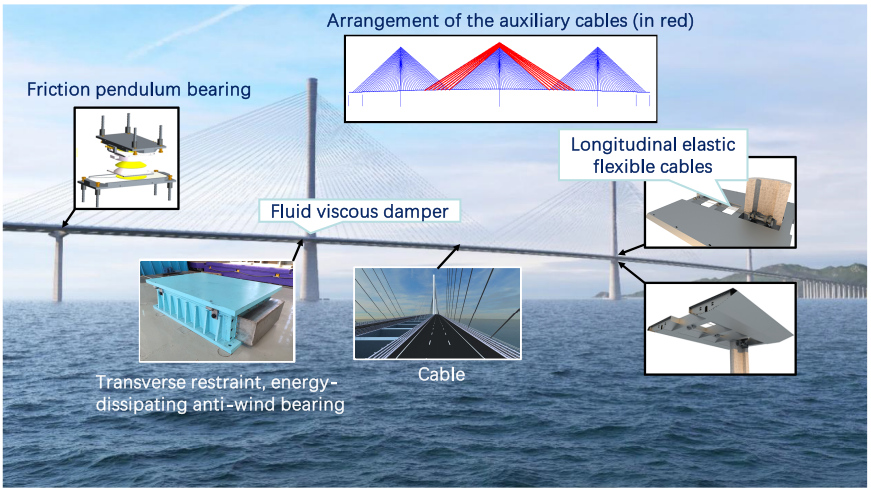

Figure 1: Effect drawing of Huangmaohai Bridge with detail.

3 Calculation Model and Parameters

3.1 Model Introduction

The bridge is configured with a span arrangement of 100 + 280 + 720 + 720 + 280 + 100 = 2200 m, forming a three-tower cable-stayed bridge with single-column towers and dual cable planes. The span-to-depth ratio is specified as 0.25, while the side-to-main span ratio is designed as 0.53. Both the side and central towers are constructed to an identical height of 263 m. And a comprehensive structural system composed of the following devices is applied to the Huangmaohai Bridge.

To improve the vertical stiffness of the bridge, five pairs of auxiliary cables are installed at the central tower, providing supplementary vertical support and contributing to better control of tower and deck deformations. Longitudinal restraint between the central tower and the girder is provided by 16 longitudinal elastic cables with a tensile strength of 1960 MPa, arranged in parallel and anchored to the top and bottom slabs of the transverse connection box. The equivalent stiffness of cables is evaluated to be $K = 6.5 \times 10^5$ kN/m. At the side towers, fluid viscous dampers are installed between the towers and girders, with four dampers per tower. The fluid viscous dampers are intended to dissipate longitudinal seismic energy and to control the relative displacement between the side towers and the girder. The damping parameters are specified as a damping coefficient C = 2500 kN/(m/s) and damping exponent $\alpha = 0.3$.

For transverse restraint, energy-dissipating anti-wind bearings are installed at the tower–girder connections of both the side and central towers. The anti-wind bearings provide transverse restraint while allowing longitudinal and vertical movements. In addition, friction pendulum bearings are installed at the transition

piers and auxiliary piers to provide seismic isolation. The friction pendulum bearings consist of longitudinal sliding plates, translational sliding plates, spherical liners, spherical bearing plates, and transverse sliding plates. The friction pendulum bearings allow horizontal sliding and provide a restoring force governed by the spherical curvature, thereby achieving seismic isolation.

These structural features, including the detailed configuration of control devices and their nonlinear mechanical characteristics, are explicitly incorporated into the finite element model. This comprehensive modeling approach enables a more realistic representation of the dynamic behavior of the bridge under extreme loading scenarios, particularly in both longitudinal and transverse directions. The general layout of the bridge is presented in Fig. 2, with the main cables in blue and the auxiliary cables in green.

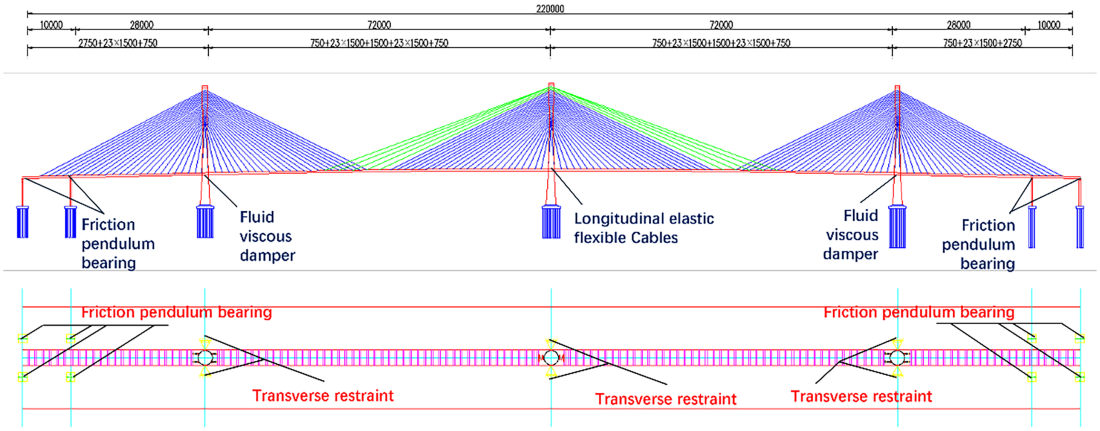

Figure 2: General layout of three-tower cable-stayed bridge (Unit: mm).

3.2 Calculate Model Parameters

3.2.1 Main Components and Materials

The towers are constructed using C60 grade concrete, while the transition piers and auxiliary piers are built with C50 grade concrete. The key mechanical properties of the various concrete grades are summarized in Table 1. The main girders are fabricated from Q345QD steel, with its principal mechanical properties provided in Table 2. The yield strength of the steel and its corresponding allowable stresses are determined according to the specifications of GB/T 714-2000, with variations based on plate thickness. The stay cables are manufactured from high-strength steel wires with a diameter of 7 mm. The elastic modulus of the cable material is specified as 195,000 MPa, while the coefficient of thermal expansion is given as 0.000012.

Table 1: Performance of concrete materials.

Concrete Grade		**C50**	**C60**
Application Structure		**Transition Piers/Auxiliary Piers**	**Cable Tower**
Mechanical properties	Elastic modulus/E (MPa)	34,500	36,000
	Shear modulus/G (MPa)	13,800	14,400
	Poisson ratio/γ	0.2	0.2
	Axial compressive design strength/MPa	22.4	27.5
	Tensile design strength/MPa	1.83	2.04

(Continued)

Table 1 (continued)

Concrete Grade Application Structure	C50 Transition Piers/Auxiliary Piers	C60 Cable Tower
Axial compressive standard strength/MPa	32.4	38.5
Tensile standard strength/MPa	2.65	2.85
Coefficient of thermal expansion/1/°C	0.000010	0.000010

Table 2: Structural steel properties.

	Q345QD
Elastic modulus/E (MPa)	210,000
Shear modulus/G (MPa)	81,000
Poisson ratio/γ	0.3
Yield strength σs (MPa)	345
Coefficient of linear expansion (1/°C)	0.000012

3.2.2 Calculation of Loads

The following load cases are considered in the analysis: (1) Permanent actions: These include the self-weight of the structure and the bridge deck pavement; (2) Highway live loads: The Highway-I grade loading standard is adopted. The bridge is designed for 8 traffic lanes, with longitudinal and transverse reduction factors as well as transverse eccentricity factors being incorporated; (3) Thermal actions: A uniform temperature increase of 27°C and decrease of −27°C are considered. Local temperature differentials are determined with reference to relevant design codes. The temperature gradient across the steel box girder section is specified according to the BS 5400 standard; (4) Wind loads: The basic design wind speed at the bridge site is determined as 46 m/s; (5) Seismic actions: The seismic design intensity is set at VII degree. Calculations are performed based on the current seismic safety evaluation report; (6) Ship collision loads: The collision forces are specified as 184 MN in the direction parallel to the water flow and 46 MN in the direction perpendicular to the water flow for both side and central towers. The acceleration response spectra for 3% damping ratios are presented in Fig. 3. Corresponding to these spectra, the Guangdong Earthquake Engineering Survey Center has provided ground acceleration time histories for two seismic intensity levels. Three horizontal acceleration time history records are provided. Based on multiple earthquake records, the vertical-to-horizontal acceleration ratio usually falls within 0.5–0.65 [30]. Although vertical and horizontal components differ in waveform, including amplitude, phase, and frequency content, adopting 0.65 as a simplified treatment remains reasonable for most conventional structural design needs; therefore, the vertical acceleration time histories are taken as 0.65 times the corresponding horizontal values. Fig. 4 shows the horizontal acceleration time history curves for E1 and E2 levels.

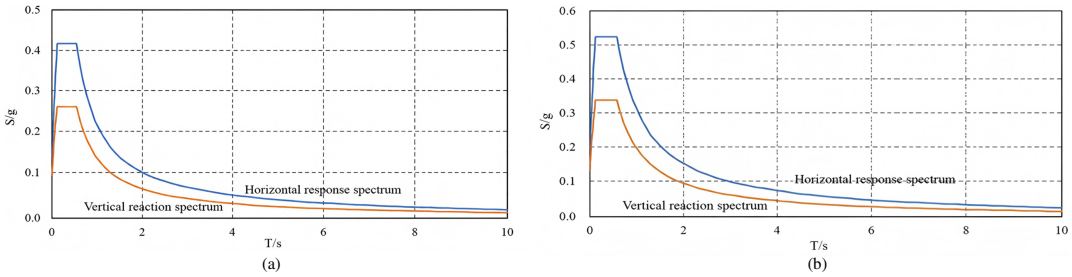

Figure 3: Damping specific acceleration response spectrum: (**a**) E1 level 3% damping specific acceleration response spectrum; (**b**) E2 level 3% damping specific acceleration response spectrum.

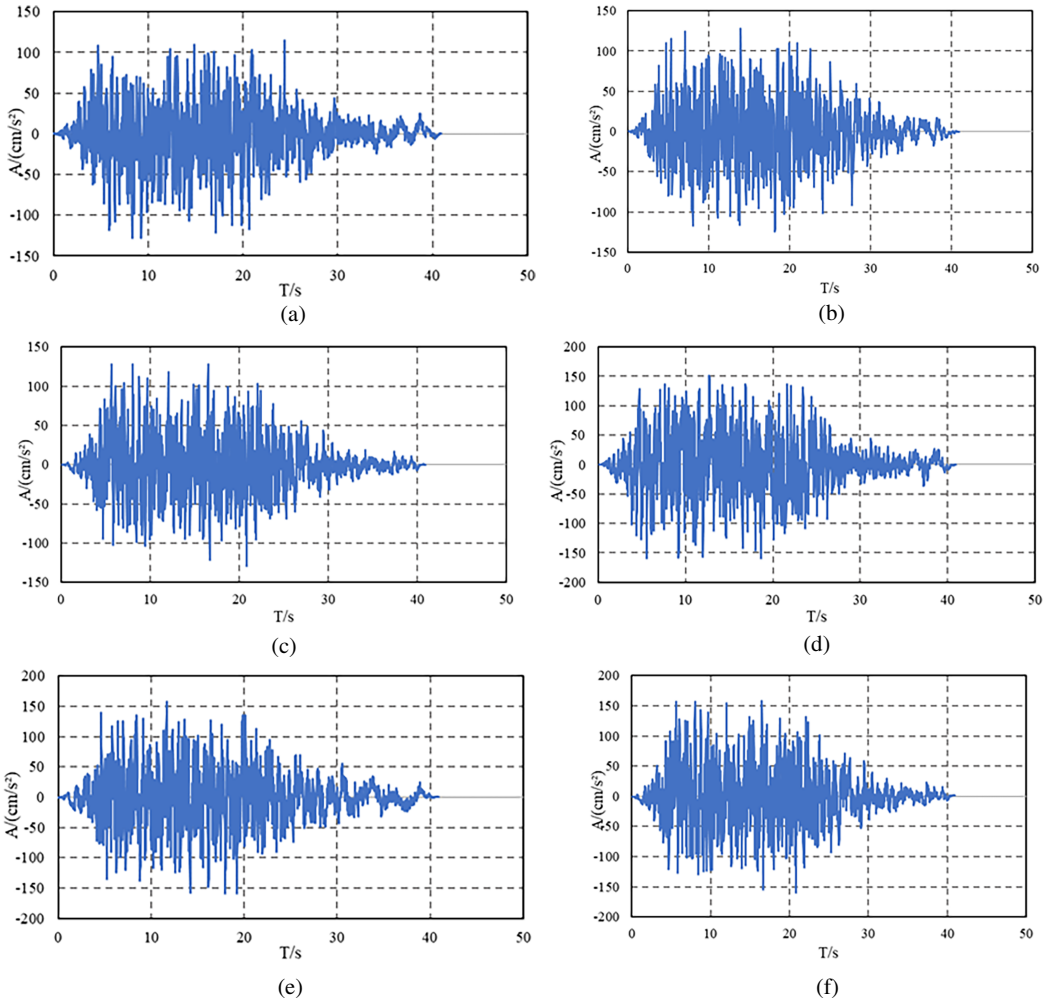

Figure 4: Horizontal acceleration time history: (**a**) The first horizontal acceleration time history at the E1 level; (**b**) The second horizontal acceleration time history at the E1 level; (**c**) The third horizontal acceleration time history at the E1 level; (**d**) The first horizontal acceleration time history at the E2 level; (**e**) The second horizontal acceleration time history at the E2 level; (**f**) The third horizontal acceleration time history at the E2 level.

3.2.3 Static and Dynamic Finite Element Model

The global static analysis of the entire bridge is performed using a spatial beam-element program. The structure is discretized based on its theoretical vertical alignment, and the internal forces and displacements

under various load cases are analyzed. The full-bridge analytical model is shown in Fig. 5, and schematic diagrams of the main tower are presented in Fig. 6. A dynamic computational model of the Huangmaohai Bridge is established using the MIDAS finite element software for seismic performance analysis. A three-dimensional finite element model is developed, where the global coordinate system is defined with the X-axis aligned with the longitudinal bridge direction, the Y-axis with the transverse direction, and the Z-axis with the vertical direction. In this model, the towers, main girder, and piers are all discretized as spatial beam elements. For the dynamic analysis, a fixed connection at the central tower is adopted. The dynamic computational model is illustrated in Fig. 7.

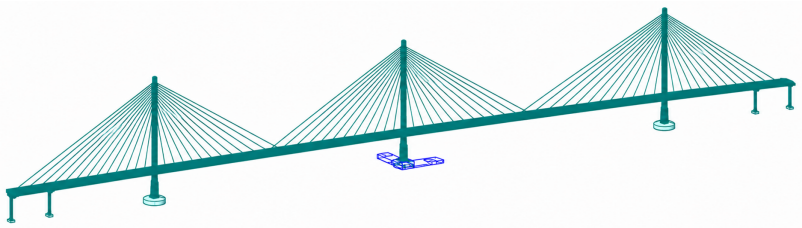

Figure 5: Static analysis model of the entire bridge.

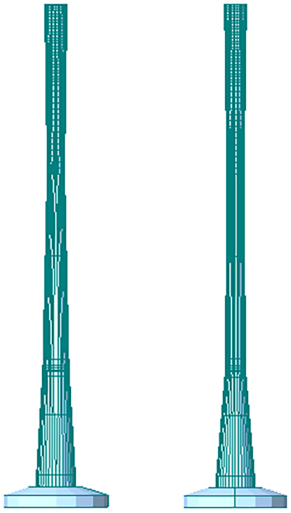

Figure 6: Schematic diagram of the main tower: (**a**) Horizontal schematic diagram of the main tower; (**b**) Longitudinal schematic diagram of the main tower.

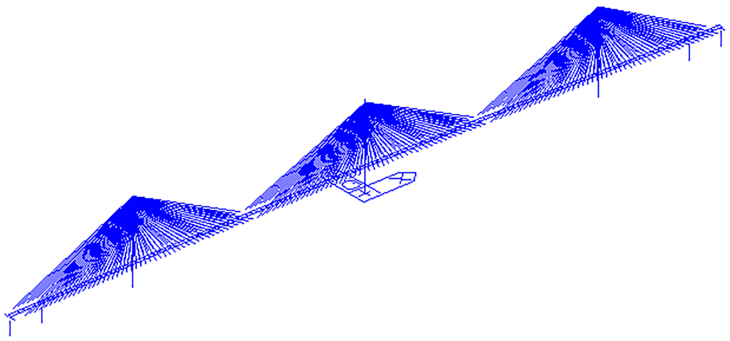

Figure 7: Dynamic calculation model.

4 Static Analysis

4.1 Displacement Calculation

In the calculation results, axial forces and stresses are defined as positive in tension and negative in compression. Based on the computational outcomes, displacement values under live loads and wind loads are summarized in Table 3. In the table, Combination 4 is constant load + live load + temperature + live load transverse wind; Combination 5 is constant load + temperature + 100-year transverse wind; Combination 6 is constant load + live load + temperature + live load longitudinal wind; and Combination 7 is constant load + temperature + 100-year longitudinal wind. The maximum vertical displacement at mid-span of the two spans of the bridge is calculated through the above combination, including both upward and downward displacements, with upward displacement considered positive and downward displacement negative. The calculated maximum displacement is then divided by the corresponding span length to obtain the deflection-to-span ratio. The envelope diagram of vertical deflections in the main girder under live loads is presented in Fig. 8. The vertical deflection-to-span ratio is calculated as 1.691/720 = 1/426, indicating that the vertical displacement satisfies the design requirements.

Table 3: Structural deformation (m).

Direction	Part	Combination	Displacement Value (m)	Amplitude Sum (m)
Vertical	Midspan	Live load	0.641/−1.076	1.691
Longitudinal	Left beam end	Combination 4	0.435/−0.727	1.162
		Combination 5	0.391/−0.705	1.096
		Combination 6	0.452/−0.744	1.196
		Combination 7	0.481/−0.796	1.277
	Right beam end	Combination 4	0.727/−0.435	1.162
		Combination 5	0.705/−0.390	1.095
		Combination 6	0.744/−0.451	1.195
		Combination 7	0.796/−0.481	1.277
	Top of the middle tower	Combination 4	0.498/−0.498	0.996
		Combination 4	0.523/−0.523	1.047
		Combination 7	0.137/−0.137	0.274

(Continued)

Table 3 (continued)

Direction	Part	Combination	Displacement Value (m)	Amplitude Sum (m)
Horizontal	Main girder at mid-span	Combination 5	0.463/−0.463	0.926
	Top of the middle Tower	Combination 5	1.935/−1.935	3.870
	Top of side tower	Combination 5	1.428/−1.428	2.856

*Note: Positive values indicate displacement toward the center span, negative values indicate displacement toward the side spans.

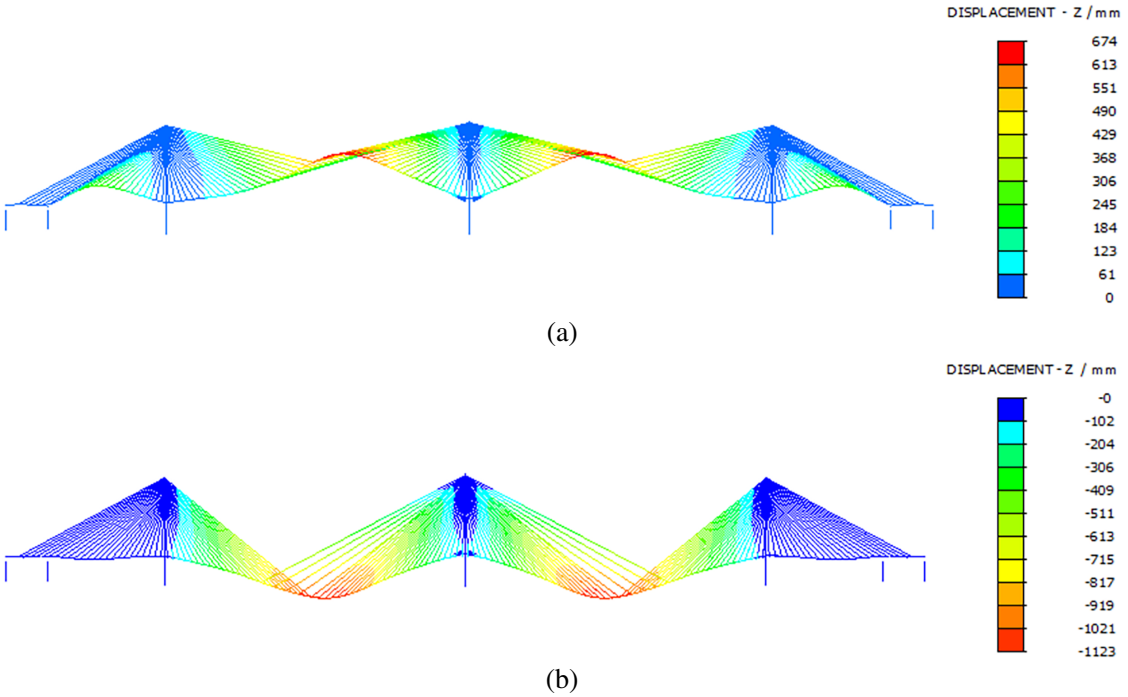

Figure 8: Envelope diagram of vertical deflection of the main beam under live load: (**a**) Maximum value; (**b**) Minimum value.

4.2 Internal Force of the Bearing

The vertical reaction forces at the bearings of the auxiliary piers and transition piers are presented in Table 4. As shown in the table, all bearings are maintained in compression without exhibiting tensile forces. Thus, the installation of tension-resistant bearings is not required. The maximum vertical reaction recorded is 1430 t. The reaction forces of the transverse wind-resistant bearings under lateral wind load are summarized in Table 5. The results demonstrate that the transverse wind-resistant bearings satisfy the design requirements. Under the most critical load combination, the wind-resistant bearings at the bridge towers are

subjected to significant forces. Specifically, the bearing at the central tower carries a load of 3200 t, presenting considerable design challenges and requiring specialized optimization in their design.

Table 4: Reaction forces of auxiliary piers and transition piers bearings (kN).

Load Combination		Auxiliary Pier Bearing	Transition Pier Bearing
Constant load		−10,964	−4573
The most unfavorable	Nmax	−14,287	−6382
	Nmin	−3412	−3675

Table 5: Reaction force at the bearing of the main tower/lateral shear force of the bearing of the pier/auxiliary pier (kN).

Load Combination	Middle Tower Bearing	Wind-Resistant Bearing for the Side Tower	Auxiliary Pier Bearing	Transition Pier Bearing
The most unfavorable	32,096	28,524	1759	1518

4.3 Stress of Steel Main Beam

The stresses at the upper and lower flanges of the steel box girder during both the bridge completion stage and operational stage are presented in Table 6. It is observed from the calculation results that the maximum stress in the steel main girder is 222 MPa, which is lower than the design strength of Q345 steel. Thus, the code requirements are satisfied. Where combination 1 is constant load (bridge formation stage); combination 2 is constant load + live load; combination 3 is constant load + live load + temperature.

Table 6: Maximum stress values of main beams under various working conditions (MPa).

Load Combinations	Upper Edge Stress		Lower Edge Stress		Strength Design Value
	MAX	MIN	MAX	MIN	
Combination 1	49	−96	47	−100	270
Combination 2	85	−138	97	−168	270
Combination 3	128	−159	177	−178	270
Combination 4	130	−161	182	−183	270
Combination 5	122	−222	114	−168	270
Combination 6	129	−159	179	−179	270
Combination 7	122	−137	102	−142	270

4.4 Stress of Stay Cables

The cable forces under the completed bridge state and the cable stresses under the most unfavorable load combinations are presented in Fig. 9 for the stay cables, and in Table 7 for the auxiliary cables. It can be observed from Fig. 9 that under the most critical combination, the maximum and minimum stresses in the stay cables are 659 and 184 MPa, respectively. The safety factors for all stay cables are verified to exceed 2.7. For the auxiliary cables, the maximum and minimum stresses are 525 and 249 MPa, respectively, with all safety factors demonstrated to be greater than 3.5.

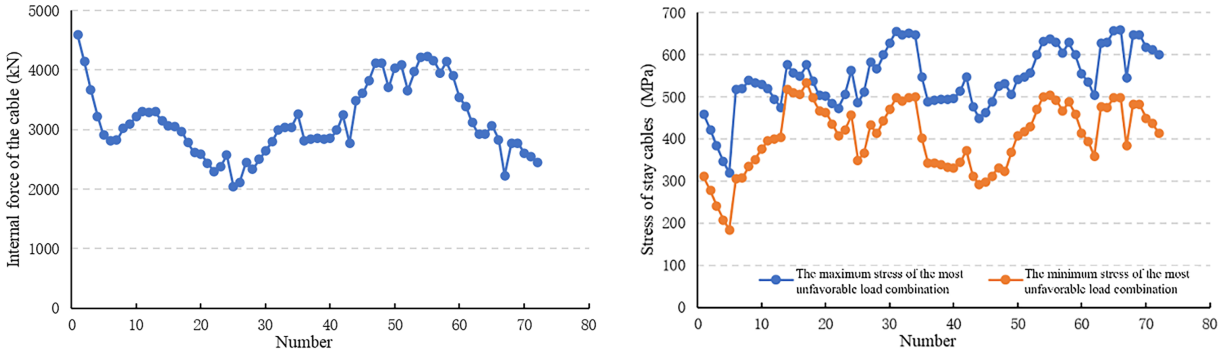

Figure 9: Cable-stayed force during the bridge formation stage: (**a**) Unloaded cable-stayed force in the bridge formation state; (**b**) The most unfavorable combination of stay cable stress.

Table 7: Auxiliary cable stress and parameter table.

Auxiliary Cable Number	Parallel Steel Wire Model	Constant Load	Most Unfavorable Combination (MPa)		Safety Factor
		Beam Ends	Max	Min	
1	7-337	309	399	414	4.7
2	7-337	305	389	249	4.8
3	7-337	312	396	256	4.7
4	7-337	382	502	270	3.7
5	7-337	397	525	301	3.5

5 Dynamic Analysis

5.1 Dynamic Characterization

Based on the established dynamic computational model, a structural dynamic characteristic analysis was conducted. The frequencies and mode shape characteristics of the first ten vibration modes of the Huangmaohai Bridge are summarized in Table 8. Graphical representations of typical vibration modes are provided in Fig. 10. When the first 150 vibration modes are considered, the mass participation factors in all directions are verified to exceed 99%, thereby meeting the code requirements. It should be noted that only the vibration modes of the main bridge are displayed in the following figures.

5.2 Internal Forces of the Tower

Based on the computational results, the internal forces in the towers of the two models are compared in Table 9. Compared with the baseline model, significant influences on the longitudinal bending moments are observed in both the side and central towers, with a more pronounced effect on the central tower. Specifically, the longitudinal bending moments at the base and deck level of the side towers are slightly reduced by approximately 22%. A reduction of about 10% is observed at the smallest cross-section. For the central tower, the longitudinal bending moment at the base is minimally reduced by only 6%. In contrast, the longitudinal bending moments at the deck level and the smallest cross-section are significantly reduced by 41%. Additionally, under the most unfavorable static loading conditions, the transverse bending moments at the critical sections of the towers are found to remain essentially unchanged compared to the baseline model.

Table 8: Dynamic characteristics of huangmaohai bridge.

Vibration Mode	Period (s)	Frequency (Hz)	Mode Shape Description
1	7.22	0.14	The central tower bends laterally
2	6.64	0.15	The towers on both sides bend in opposite directions
3	6.56	0.15	The two towers bend in the same direction
4	6.33	0.16	The main beam is opposed to vertical bending
5	5.07	0.20	The main beam is opposed to symmetrical transverse bending
6	3.93	0.25	The entire bridge is opposed to longitudinal bending
7	3.81	0.26	The main beam is vertically curved in a symmetrical pattern
8	3.60	0.28	The main beam is symmetrically bent horizontally
9	3.19	0.31	The main beam is opposed to vertical bending
10	2.68	0.37	The main beam is vertically curved in a symmetrical pattern

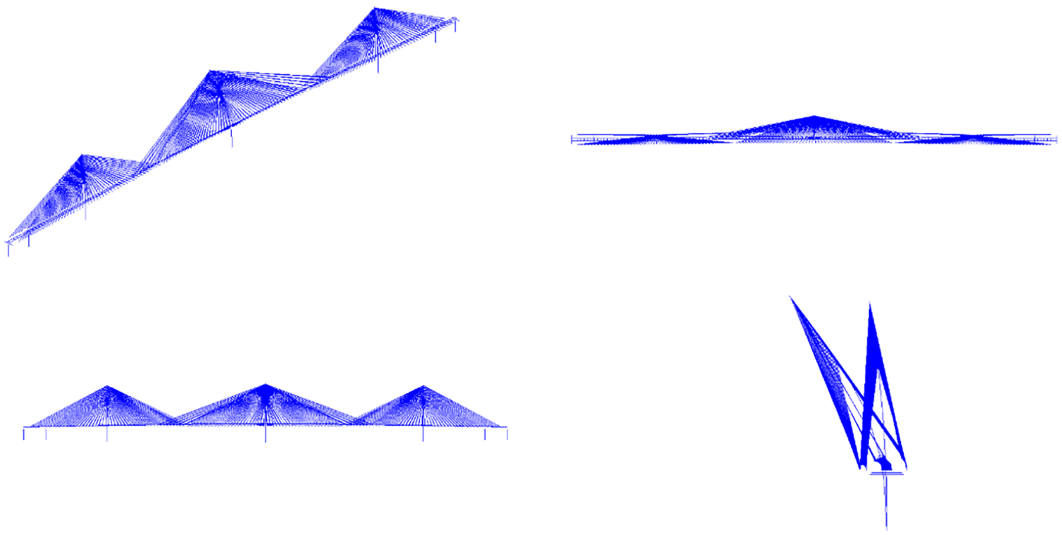

Figure 10: First-order mode shape diagram (Period: 7.22 s).

Table 9: Comparison of internal forces of the tower.

Part		Basic Model		Comprehensive Model	
		M2	M3	M2	M3
Side tower	The bottom of the tower	4,195,836	2,066,681	4,213,207	1,601,900
	At the bridge deck	1,765,224	1,371,159	1,771,162	1,048,130
	The finest part	596,832	434,964	594,995	392,457
Middle tower	The bottom of the tower	5,761,578	2,931,586	5,775,038	2,749,722
	At the bridge deck	2,290,835	1,771,044	2,317,514	1,070,898
	The finest part	815,610	463,357	839,056	269,272

5.3 Seismic Response Comparison

Under the seismic events E1 and E2, the calculation differences between the baseline model and the comprehensive model are compared. The seismic responses of the key sections of the bridge towers in both models are summarized in the following Tables 10 and 11. As indicated in Tables 10 and 11, the internal forces at critical sections are generally reduced in the comprehensive model compared to the benchmark model under both E1 and E2 seismic actions. Under combined longitudinal-vertical seismic excitation, reductions ranging from 23% to 54% are observed at most critical sections, except at the deck level of the side towers where the reduction is relatively modest. For transverse-vertical seismic excitation, more significant reductions are achieved at the pile cap bottom and tower base sections. The side towers experience approximately 20% reduction at both the tower base and pile cap bottom, while the central tower demonstrates approximately 30% reduction at these locations. However, smaller reductions are observed at the deck level and the minimum cross-section. At the central tower, the bending moments at these sections are reduced by only about 4% under E1 seismic action. Similarly, at the minimum cross-section of the side towers, the bending moment reduction is merely 2% under E2 seismic action. For other loading conditions, these two sections demonstrate reduction rates between 15% and 29%. According to Tables 12 and 13, the tower top displacements are found to be essentially identical between the two models under transverse-vertical seismic excitation, with minimal variations in girder end displacements. However, under longitudinal-vertical seismic excitation, the girder end displacements are substantially reduced by approximately 20% in the comprehensive model.

Table 10: Seismic responses at key sections under longitudinal + vertical seismic excitation (kN·m).

Item		Benchmark Model		Comprehensive Model	
		E1	E2	E1	E2
Side Tower	Pile Cap Bottom	1,456,921	2,531,942	1,128,864	1,653,270
	Tower Base	1,071,352	1,512,561	1,028,751	1,536,224
	Deck Level	740,725	1,001,222	369,753	555,168
	Minimum Section	516,868	587,292	243,704	321,900
Central Tower	Pile Cap Bottom	4,720,017	7,925,594	2,618,370	3,644,434
	Tower Base	4,128,801	6,599,261	2,418,600	3,256,409
	Deck Level	935,411	985,287	699,179	511,765
	Minimum Section	460,258	616,085	276,999	438,555

Table 11: Seismic responses at key sections under transverse + vertical seismic excitation (kN·m).

Item		Benchmark Model		Comprehensive Model	
		E1	E2	E1	E1
Side Tower	Pile Cap Bottom	2,865,819	4,119,672	2,310,252	3,023,279
	Tower Base	2,357,881	3,338,494	2,059,209	2,678,831
	Deck Level	960,022	1,408,411	866,937	1,004,238
	Minimum Section	606,345	719,463	431,424	704,761

(Continued)

Table 11 (continued)

Item		Benchmark Model		Comprehensive Model	
		E1	E2	E1	E1
Central Tower	Pile Cap Bottom	2,915,038	5,091,612	2,226,472	3,020,805
	Tower Base	2,470,247	4,163,215	2,086,136	2,721,070
	Deck Level	1,046,735	1,771,731	1,034,488	1,476,114
	Minimum Section	598,906	901,257	563,578	766,098

Table 12: Displacements at key points under longitudinal + vertical seismic excitation (m).

Key Point	Benchmark Model		Comprehensive Model	
	E1	E2	E1	E2
East Girder End	0.151	0.243	0.128	0.191
West Girder End	0.153	0.266	0.135	0.198
Side Tower Top	0.197	0.296	0.176	0.277
Central Tower Top	0.200	0.283	0.143	0.264

Table 13: Displacements at key points under transverse + vertical seismic excitation (m).

Key Point	Benchmark Model		Comprehensive Model	
	E1	E2	E1	E2
East Girder End	0.057	0.078	0.058	0.080
West Girder End	0.186	0.250	0.187	0.255
Side Tower Top	0.600	0.845	0.605	0.850
Central Tower Top	0.913	1.159	0.919	1.168

6 Conclusion

This study systematically investigates the static and dynamic structural behavior of the Huangmao Sea Bridge through refined finite element modeling. It explores the contributions of critical structural components, including the elastic restraints of the central tower, the dampers of the side towers, and the transverse seismic isolation system, in structural modeling and response analysis. The findings contribute to innovative approaches in seismic design and structural optimization of long-span sea-crossing bridges. The main conclusions are summarized as follows:

(1) The static performance is verified to satisfy code requirements. Under static load combinations, the maximum stress in the main girder is controlled at 222 MPa, which remains below the design strength of Q345 steel. The vertical deflection-to-span ratio is determined as 1/426, confirming adequate stiffness compliance. The safety factors for stay cables and auxiliary cables exceed 2.7 and 3.5 respectively, demonstrating that the overall structure is confirmed to be within the safe range. These results not only validate the structural design but also provide a refined reference for the static performance evaluation of long-span sea-crossing bridges with similar configurations.

(2) The comprehensive structural system is demonstrated to significantly improve seismic performance. Compared with the benchmark model, the internal forces at critical tower sections are generally reduced under both E1 and E2 seismic events. Under longitudinal-vertical seismic excitation, bending moment reductions of 23%–54% are achieved at key sections of both side and central towers. Under transverse-vertical excitation, the bending moments at tower bases are reduced by 20% and 30% for side and central towers respectively, demonstrating effective seismic mitigation. These results highlight the effectiveness of the proposed system in mitigating seismic impacts and offer valuable insights for the seismic optimization of long-span cable-stayed bridges.

(3) Significant displacement control is achieved through the integrated structural measures. Under longitudinal-vertical seismic excitation, the end displacements of the main girder are reduced by approximately 20% in the comprehensive model, with similar reductions observed at the tops of the towers. The overall structural displacement response is effectively suppressed, demonstrating the effectiveness of the implemented damping and restraint systems. These findings validate the proposed control strategy and offer practical guidance for enhancing the seismic resilience of long-span bridges.

While this study provides valuable insights into the seismic performance of long-span sea-crossing cable-stayed bridges, certain shortcomings remain. For instance, the current analysis focuses primarily on the structural response under idealized boundary conditions and simplified damping models. This research lays the groundwork for future research. Subsequent studies will focus on the development of key energy dissipation and restraint devices tailored for multi-tower, ultra-long-span sea-crossing cable-stayed bridges, as well as the investigation of critical parameters influencing energy dissipation and restraint strategies. These efforts aim to further enhance the seismic resilience and design precision of complex bridge systems.

Acknowledgement: Not applicable.

Funding Statement: This research is bearinged by the China Communications Construction Technology research project (YSZX-03-2022-01-B). The authors express sincere appreciation for their contributions to this research.

Author Contributions: The authors confirm contribution to the paper as follows: Conceptualization, Dawei Shen and Xiang Chen; methodology, Yuanyin Song and Yaoyu Zhu; software, Deyun Liu and Rong Lv; validation, Yaoyu Zhu, Rong Lv and Wen-Wei Wang; formal analysis, Dawei Shen, Yaoyu Zhu, Yuanyin Song and Deyun Liu; investigation, Xiang Chen and Rong Lv; resources, Dawei Shen; data curation, Dawei Shen and Xiang Chen; original draft preparation, Yuanyin Song, Deyun Liu; writing—review and editing, Yaoyu Zhu and Wen-Wei Wang; visualization, Rong Lv; supervision, Yuanyin Song and Yaoyu Zhu; project administration, Dawei Shen and Xiang Chen; funding acquisition, Dawei Shen and Xiang Chen. All authors reviewed and approved the final version of the manuscript.

Availability of Data and Materials: Data available on request from the authors. The data that bearing the findings of this study are available from the Corresponding Author, [Yuanyin Song], upon reasonable request.

Ethics Approval: This study was conducted in accordance with institutional ethical guidelines. No human subject was involved.

Conflicts of Interest: The authors declare no conflicts of interest.

References

1. Cui B, Wu H, Wei L, Guo Z, Ma Z. Pursuit for industrialized construction of Nanjing Jiangxinzhou Yangtze River bridge. Struct Eng Int. 2022;32(2):252–60. doi:10.1080/10168664.2021.1955086.
2. Liang D, Yao CR, Liu SZ. Structural type selection for long-span bridges in mountain area. Appl Mech Mater. 2012;256–259:1596–600. doi:10.4028/www.scientific.net/amm.256-259.1596.

3. Gao Z, Xu W, Mei X, Zhang Y, Huo X. Key construction technology of HuSuTong Yangtze River bridge. Struct Eng Int. 2023;33(1):84–8. doi:10.1080/10168664.2021.1991252.
4. Calvi GM, Sullivan TJ, Villani A. Conceptual seismic design of cable-stayed bridges. J Earthq Eng. 2010;14(8):1139–71. doi:10.1080/13632469.2010.505275.
5. Zhang L, Qiu G, Chen Z. Structural health monitoring methods of cables in cable-stayed bridge: a review. Measurement. 2021;168(4):108343. doi:10.1016/j.measurement.2020.108343.
6. Lu Y, Huo X, Qu G, Li Y, Wang L. Cable-stayed bridge model updating based on response surface method. Struct Durab Health Monit. 2025;19(4):919–35. doi:10.32604/sdhm.2025.062537.
7. Liang Y, Kong YZ, Yan L, Zhao ZH, Guan PW. Multi-hazard fragility analysis of cross-sea cable-stayed bridges cable bent tower under seismic-wind combined action. Soil Dyn Earthq Eng. 2025;195(1):109422. doi:10.1016/j.soildyn.2025.109422.
8. Cheng Y, Wang W, Zhu Z, Zhong Y, Tang Y. Impact resistance for ECC-RC bridge columns protected by an innovative steel-GFRP-foam anti-collision device: experimental, numerical and theoretical analysis. Compos Struct. 2025;373:119667. doi:10.1016/j.compstruct.2025.119667.
9. Qian C, Zhu L, Zhu Q, Ding Q, Yan L. Pattern and mechanism of wind-induced static instability of super-long-span cable-stayed bridge under large deformation. J Wind Eng Ind Aerodyn. 2022;221:104910. doi:10.1016/j.jweia.2022.104910.
10. Li JA, Feng D. Fatigue life evaluation of bridge stay cables subject to monitoring traffic and considering road roughness. Eng Struct. 2023;293(2):116572. doi:10.1016/j.engstruct.2023.116572.
11. Zhang W, Wang W, Tang Y, Sun K, Zhou C. Explainable machine learning driven strength degradation investigation of BFRP bar in seawater and sea sand concrete environment. Structures. 2025;71:108205. doi:10.1016/j.istruc.2025.108205.
12. Lu X, Wei K, Deng K, Xu L. Lifetime seismic resilience assessment of a sea-crossing cable-stayed bridge exposed to long-term scour and corrosion. Ocean Eng. 2024;295(6):116990. doi:10.1016/j.oceaneng.2024.116990.
13. Gimsing NJ, Georgakis CT. Cable bearinged bridges: concept and design. 3rd ed. New York, NY, USA: John Wiley & Sons; 2012.
14. Cui B, Wu H, Zhao C, Liu J, Guo Z. Steel-concrete composite cable-stayed bridge—main bridge of the Jiangxinzhou Yangtze River bridge at Nanjing. Struct Eng Int. 2023;33(1):107–14. doi:10.1080/10168664.2021.1999191.
15. Wang Y, Wu Z, Zhang K, Wang Y. Study on the mechanical performance of wet concrete joints in large-span composite steel-concrete cable-stayed bridges. Struct Durab Health Monit. 2025;19(3):613–42. doi:10.32604/sdhm.2024.058451.
16. Mary A, Joseph A. Seismic performance evaluation of cable-stayed suspension bridge. In: Proceedings of SECON'24. Cham, Switzerland: Springer Nature; 2024. p. 1199–212. doi:10.1007/978-3-031-70431-4_89.
17. Li Y, Sun Z, Mangalathu S, Li Y, He W, Xue X. Machine learning-based full-life-cycle seismic response assessment for in-service bridge piers: comprehensive analysis of interpretability and seismic fragility. Structures. 2025;80:110050. doi:10.1016/j.istruc.2025.110050.
18. Ruiz-Teran AM, Aparicio AC. Structural behaviour and design criteria of under-deck cable-stayed bridges and combined cable-stayed bridges. Part 2: multispan bridges. Can J Civ Eng. 2008;35(9):951–62. doi:10.1139/l08-034.
19. Huang Q, Wang WW, Tang Y, Guo K, Zhou C. Failure modes analysis of reinforced concrete beams under impact loads based on machine learning and SHAP approach. Eng Fail Anal. 2026;183:110281. doi:10.1016/j.engfailanal.2025.110281.
20. Chai SB, Li LH, Wang XL. Study on asymmetric arrangement ratio of main span stay cables of multi-tower cable-stayed bridge. Structures. 2024;64(2):106539. doi:10.1016/j.istruc.2024.106539.
21. Guo W, Li J, Guan Z. Shake table test on a long-span cable-stayed bridge with viscous dampers considering wave passage effects. J Bridge Eng. 2021;26(2):04020118. doi:10.1061/(asce)be.1943-5592.0001665.
22. Tan M, Bai Z, Chen D. Comparative research of extra-large-span cable-stayed bridge with steel truss girder and steel box girder. MATEC Web Conf. 2015;25:04002. doi:10.1051/matecconf/20152504002.
23. Zhang XJ. Investigation on mechanics performance of cable-stayed-suspension hybrid bridges. Wind Struct. 2007;10(6):533–42. doi:10.12989/was.2007.10.6.533.

24. Sun HH. Research on significant influencing factors and intelligent prediction of long-term performance of cable-stayed bridges [dissertation]. Shanghai, China: Tongji University; 2020. (In Chinese).
25. Sun H, Chen W, Guo X, Cai S. Intelligent recurrence and prediction of long-term mechanical properties of in-service cable-stayed bridges with ambient temperature and concrete time-dependent effects. J Civ Struct Health Monit. 2022;12(3):659–73. doi:10.1007/s13349-022-00573-5.
26. Cheng Y, Wang W, Wu Z, Tang Y, Zhao Q, Zhang J. Crashworthiness analysis of a novel steel-GFRP-foam protective structure for ECC-RC pier against vessel collision. Ocean Eng. 2025;340:122299. doi:10.1016/j.oceaneng.2025.122299.
27. Hiroshi N, Toshiyuki K, Ryoichi O, Toshiyuki N. Elastic plastic and finite displacement analysis of cable stayed bridge. Mem Fac Eng. 1985;26:251–71.
28. Qiu J, Shen RL, Li HG, Zhang X. Analysis of structural parameters of cable-stayed suspension bridges. Adv Mater Res. 2010;163–167:2068–76. doi:10.4028/www.scientific.net/amr.163-167.2068.
29. Xu K, Li M, Ma R, Han Q, Du X. Analytical optimization and performance evaluation of tuned inerter-negative-stiffness dampers (TINSD) for seismic response control in long-span bridges with floating systems (LBFSs). Earthq Engng Struct Dyn. 2025;54(11):2784–804. doi:10.1002/eqe.70001.
30. Li J, Jia P, Cheng H. Response spectrum and computational analysis of vertical earthquake acceleration for frame structures. China New Technol Prod. 2013;(1):186. (In Chinese).